Article

Cell Metabolism

Glutamine Metabolism Regulates Proliferation and Lineage Allocation in Skeletal Stem Cells

Graphical Abstract

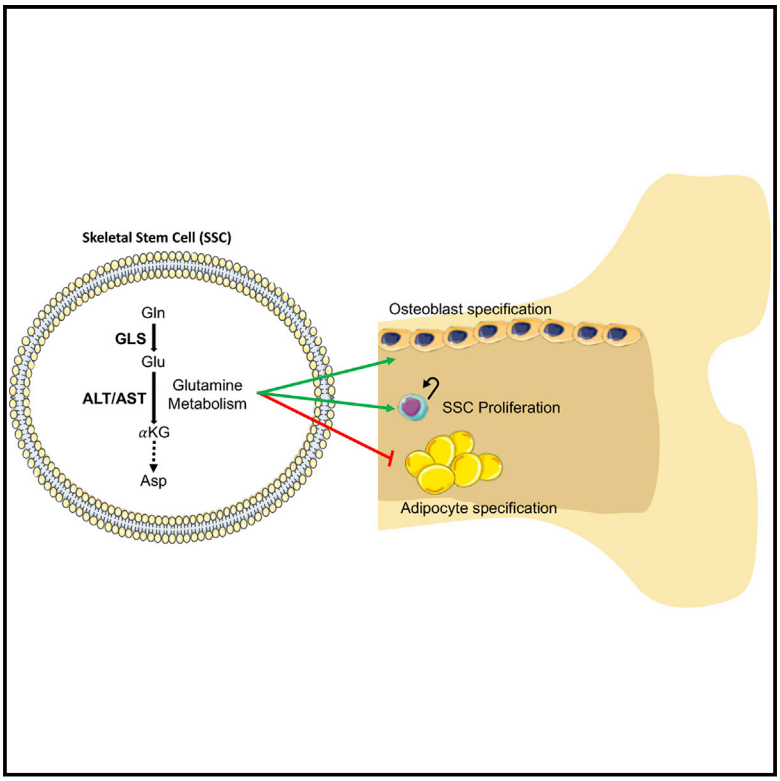

Authors

Yilin Yu, Hunter Newman, Leyao Shen, ..., Guo-Fang Zhang, Matthew J. Hilton, Courtney M. Karner

Correspondence

courtney.karner@duke.edu

In Brief

Skeletal stem cells (SSCs) provide a reservoir of bone-forming osteoblasts throughout life. Yu et al. investigate glutamine metabolism in SSCs. Glutamine-derived α-ketoglutarate supports amino acid biosynthesis and proliferation in SSCs. Inhibiting glutamine metabolism in SSCs results in low bone mass and increased marrow adiposity in mice.

Highlights

- Skeletal stem cells increase glutamine metabolism during osteoblast differentiation
- Glutamine metabolism regulates osteoblast and adipocyte specification
- Mice unable to metabolize glutamine have less bone and increased marrow fat
- Amino acid transaminase-derived α-ketoglutarate is critical for SSC proliferation

Yu et al., 2019, Cell Metabolism *29*, 966–978
April 2, 2019
https://doi.org/10.1016/j.cmet.2019.01.016

CellPress

CellPress

Cell Metabolism
Article

Glutamine Metabolism Regulates Proliferation and Lineage Allocation in Skeletal Stem Cells

Yilin Yu,[1] Hunter Newman,[1] Leyao Shen,[1] Deepika Sharma,[1] Guoli Hu,[1] Anthony J. Mirando,[1] Hongyuan Zhang,[1] Everett Knudsen,[1] Guo-Fang Zhang,[2,3] Matthew J. Hilton,[1,4] and Courtney M. Karner[1,4,5,*]

[1]Department of Orthopaedic Surgery, Duke Orthopaedic Cellular, Developmental, and Genome Laboratories, Duke University School of Medicine, Durham, NC 27710, USA

[2]Sarah W. Stedman Nutrition and Metabolism Center & Duke Molecular Physiology Institute, Duke University Medical Center, 300 North Duke Street, Durham, NC 27701, USA

[3]Department of Medicine, Duke University School of Medicine, Durham, NC 27701, USA

[4]Department of Cell Biology, Duke University, Durham, NC 27710, USA

[5]Lead Contact

*Correspondence: courtney.karner@duke.edu

https://doi.org/10.1016/j.cmet.2019.01.016

SUMMARY

Skeletal stem cells (SSCs) are postulated to provide a continuous supply of osteoblasts throughout life. However, under certain conditions, the SSC population can become incorrectly specified or is not maintained, resulting in reduced osteoblast formation, decreased bone mass, and in severe cases, osteoporosis. Glutamine metabolism has emerged as a critical regulator of many cellular processes in diverse pathologies. The enzyme glutaminase (GLS) deaminates glutamine to form glutamate—the rate-limiting first step in glutamine metabolism. Using genetic and metabolic approaches, we demonstrate GLS and glutamine metabolism are required in SSCs to regulate osteoblast and adipocyte specification and bone formation. Mechanistically, transaminase-dependent α-ketoglutarate production is critical for the proliferation, specification, and differentiation of SSCs. Collectively, these data suggest stimulating GLS activity may provide a therapeutic approach to expand SSCs in aged individuals and enhance osteoblast differentiation and activity to increase bone mass.

INTRODUCTION

Osteoporosis is a prevalent human disease characterized by low bone mass and deterioration of the bone microarchitecture, resulting in increased fracture susceptibility (Eisman et al., 2012; U.S. Department of Health and Human Services, 2004). Osteoporosis affects approximately 10 million Americans over the age of 50 and is estimated to cost upwards of 20 billion dollars per annum (Becker et al., 2010). Adult bone is a dynamic tissue undergoing constant remodeling, which is regulated by both the number and cellular activity of the bone-forming osteoblasts and bone-resorbing osteoclasts. Skeletal stem cells (SSCs), also termed bone marrow mesenchymal stromal cells (BMSCs), are critical regulators of postnatal bone homeostasis by providing a reservoir of osteoblasts throughout life (Bianco and Robey, 2015; Mizoguchi et al., 2014; Zhou et al., 2014). Originally, SSCs were defined by multiple characteristics, including adherence to plastic, ability to generate fibroblastic colonies (CFU-F) in culture, and the capability to differentiate into adipocytes, osteoblasts, and chondrocytes *in vitro* (Bianco and Robey, 2015; Owen and Friedenstein, 1988; Friedenstein et al., 1966). Recent studies have demonstrated SSCs arise postnatally, are tightly associated with the vasculature *in vivo*, and can be targeted in mouse using various Cre lines, including *Prx1Cre* and *LeprCre* (Mizoguchi et al., 2014; Zhou et al., 2014; Ding and Morrison, 2013; Greenbaum et al., 2013). Under normal physiological conditions, SSCs are quiescent but rapidly proliferate and can differentiate into adipocytes, osteoblasts, and chondrocytes in response to injury (Zhou et al., 2014; Park et al., 2012). With age, SSC numbers decline. This results in decreased osteoblast generation, leading to decreased bone mass and diminished regeneration potential over time. Moreover, the differentiation potential of SSCs shifts to favor adipogenesis with age, further decreasing osteoblast generation and bone formation (Moerman et al., 2004; Justesen et al., 2001; D'Ippolito et al., 1999; Nishida et al., 1999). Recent studies have identified many extrinsic signals that regulate SSC lineage commitment and differentiation (Fairfield et al., 2018; Balani et al., 2017; Fan et al., 2017; Wu et al., 2017; Yue et al., 2016; Li et al., 2013). However, the intrinsic mechanisms governing SSC commitment to the osteogenic rather than adipogenic lineage remain to be elucidated.

Glutamine metabolism is emerging as an intriguing regulatory node frequently altered in many pathological conditions (Still and Yuneva, 2017; Zhang et al., 2017; Karner et al., 2015). Glutamine is the most abundant non-essential amino acid in circulation and has multiple metabolic uses in the cell (Stein and Moore, 1954). Glutamine metabolism is initiated by the enzyme glutaminase (GLS), which deaminates it to form glutamate, an important intermediate metabolite that has many biosynthetic uses in the cell. The physiological role of glutamine metabolism during embryonic and postnatal development is unknown as mice deficient for *Gls* die within 24 h of birth because of defects in glutamatergic neural transmission (Masson et al., 2006). However, no other phenotypes were reported in these mice, suggesting glutamine

metabolism is not important physiologically. On the contrary, much is known about the importance of glutamine metabolism in pathological conditions. For example, some tumor cells utilize glutamine metabolism to provide NADPH and better utilize glucose carbons to generate biomass (DeBerardinis et al., 2007). In other tumors, glutamine metabolism provides carbon for lipid and glutathione (GSH) biosynthesis as well as nitrogen for nucleotide biosynthesis to control oxidative stress and support proliferation (Le et al., 2012; Metallo et al., 2011; Mullen et al., 2011; Wise et al., 2011; Wise and Thompson, 2010; DeBerardinis et al., 2007). It is unknown if SSCs utilize glutamine metabolism, and if so, what it is used for.

Here, we define the role of glutamine metabolism during physiological bone formation and homeostasis. We describe the distinct requirement for glutamine metabolism in SSCs to maintain bone homeostasis. Using genetic and metabolic approaches, we demonstrate GLS activity and glutamine metabolism regulate SSC proliferation and appropriate lineage allocation in mice. Collectively, our data highlight the previously unknown role for glutamine metabolism in SSCs regulating physiological bone formation.

RESULTS

Differential Requirements for Glutamine Metabolism during Mesenchymal Stem Cell Differentiation

Upon examination of the metabolic needs of SSCs in culture, we observed a significant increase in glutamine consumption during osteoblast differentiation (Figures 1A, 1C, and S1A). Likewise, GLS activity was markedly increased during osteoblast differentiation (Figure 1D). Conversely, during adipocyte differentiation, neither glutamine consumption nor GLS activity were altered relative to undifferentiated SSCs (Figures 1B–1D and S1B). To determine if exogenous glutamine is required for SSC differentiation, we cultured SSCs under osteogenic or adipogenic conditions in the presence or absence of glutamine supplementation. SSCs underwent robust differentiation into either osteoblast or adipocyte lineages when cultured in the presence of exogenous glutamine (Figures 1E, 1F, S1C, and S1D). Glutamine withdrawal reduced SSC differentiation into the osteoblast lineage as exemplified by reduced matrix mineralization and decreased marker gene expression (Figures 1E and S1C). Conversely, glutamine withdrawal increased adipocyte marker gene expression and lipid accumulation during adipocyte differentiation (Figures 1F and S1D). These data suggest SSCs utilize glutamine disparately during differentiation into osteoblast and adipocyte lineages.

GLS is the primary enzyme responsible for glutamine catabolism. GLS activity is encoded by two protein isoforms, kidney-type glutaminase A (KGA, encoded by *Gls*) and liver-type glutaminase (LGA, encoded by *Gls2*). qPCR analyses demonstrated that SSCs express *Gls* at much higher levels than *Gls2* in both the undifferentiated and differentiated conditions (Figures 1G and S1E). Moreover, *Gls2* expression was negligible, suggesting *Gls* encodes the majority of GLS activity in SSCs. To test this hypothesis, we inhibited KGA using the small molecule inhibitor Bis-2-(5-phenylacetamido-1,3,4-thiadiazol-2-yl)ethyl sulfide (BPTES) (Thangavelu et al., 2012). BPTES treatment significantly reduced ^{3}H-glutamate production from L-[2,3,4-^{3}H] glutamine, confirming *Gls* encodes the primary GLS isoform expressed in SSCs (Figure 1H).

We next sought to understand how glutamine is utilized during osteoblast differentiation. First, we determined the effect of GLS inhibition on downstream metabolites using mass spectrometry. GLS inhibition significantly diminished intracellular glutamate and α-ketoglutarate (αKG) as well as the downstream products aspartate and alanine (Figure 1I). Conversely, GLS inhibition had no effect on other products of glutamine metabolism (e.g., proline) (Figure 1I). Next, we used stable isotopically labeled glutamine to trace the relative metabolic fluxes of glutamine. Briefly, SSCs precultured in growth or osteogenic media for 7 days were incubated with a glutamine tracer uniformly labeled with ^{13}C ([U-^{13}C]glutamine) for 1 h and contribution of the tracer to downstream metabolites was determined by measuring the mass isotope-labeling pattern (Figure 1J). As a control, SSCs were cultured in BPTES for 1 h prior to the 1-h incubation with [U-^{13}C]glutamine. As expected, a significant amount of glutamate was derived from glutamine (Figures 1K and S1F). Likewise, glutamine carbon contributed to the tricarboxylic acid (TCA) cycle (e.g., citrate) and was used for amino acid (e.g., proline, aspartate, and alanine) and GSH biosynthesis (Figures S1G–S1J). Importantly, glutamine contribution to citrate, amino acid, and GSH biosynthesis was prevented by BPTES treatment (Figures S1F–S1J). We next evaluated glutamine metabolism in SSCs during osteoblast differentiation. Glutamine contributed to citrate both through oxidation (M+4) and reductive carboxylation (M+5) in undifferentiated SSCs (Figure 1L). Glutamine contribution to citrate (both M+4 and M+5) was significantly reduced in differentiated SSCs (Figure 1L). This is likely the result of higher glucose flux associated with osteoblast differentiation, which dilutes the labeling from glutamine. Conversely, glutamine contribution to aspartate and other amino acids remained consistent during differentiation (Figures 1M and S1M). These data suggest that in differentiated SSCs, glutamine carbon is used primarily to provide αKG, which contributes to amino acid biosynthesis in SSCs.

Gls Is Required for Bone Formation *In Vivo*

To determine the role of *Gls* during bone formation directly, we deleted a conditionally null (floxed) allele of *Gls* (*Gls^{fl}*) in the mesenchymal progenitor cells of the limb bud using the *Prx1Cre* deleter mouse (Masson et al., 2006; Logan et al., 2002). *Prx1Cre* is expressed throughout the limb bud mesenchyme, beginning at embryonic day 9.5 and is expressed in chondrocytes and during all stages of osteoblast differentiation (Figures S2A and S2E). *Prx1Cre;Gls$^{fl/fl}$* mice were born at Mendelian ratios and were indistinguishable from wild-type littermates at birth despite loss of GLS protein expression (Figures S2B–S2D). X-ray analyses of 4-month-old mice demonstrate the long bones from *Prx1Cre;Gls$^{fl/fl}$* mice are overtly normal with no defects in length, growth, or morphology relative to wild-type littermates (Figure S2F). These analyses did identify a reduction in overall bone mass in *Prx1Cre;Gls$^{fl/fl}$* mice relative to wild-type littermates (Figure S2F). Microscopic computed tomography (μCT) analyses confirmed that *Gls* deletion resulted in a significant reduction in bone mass (Figures 2A and 2B). Quantification of the μCT analyses demonstrated that *Gls* deletion resulted in significant reductions in trabecular bone volume per tissue volume

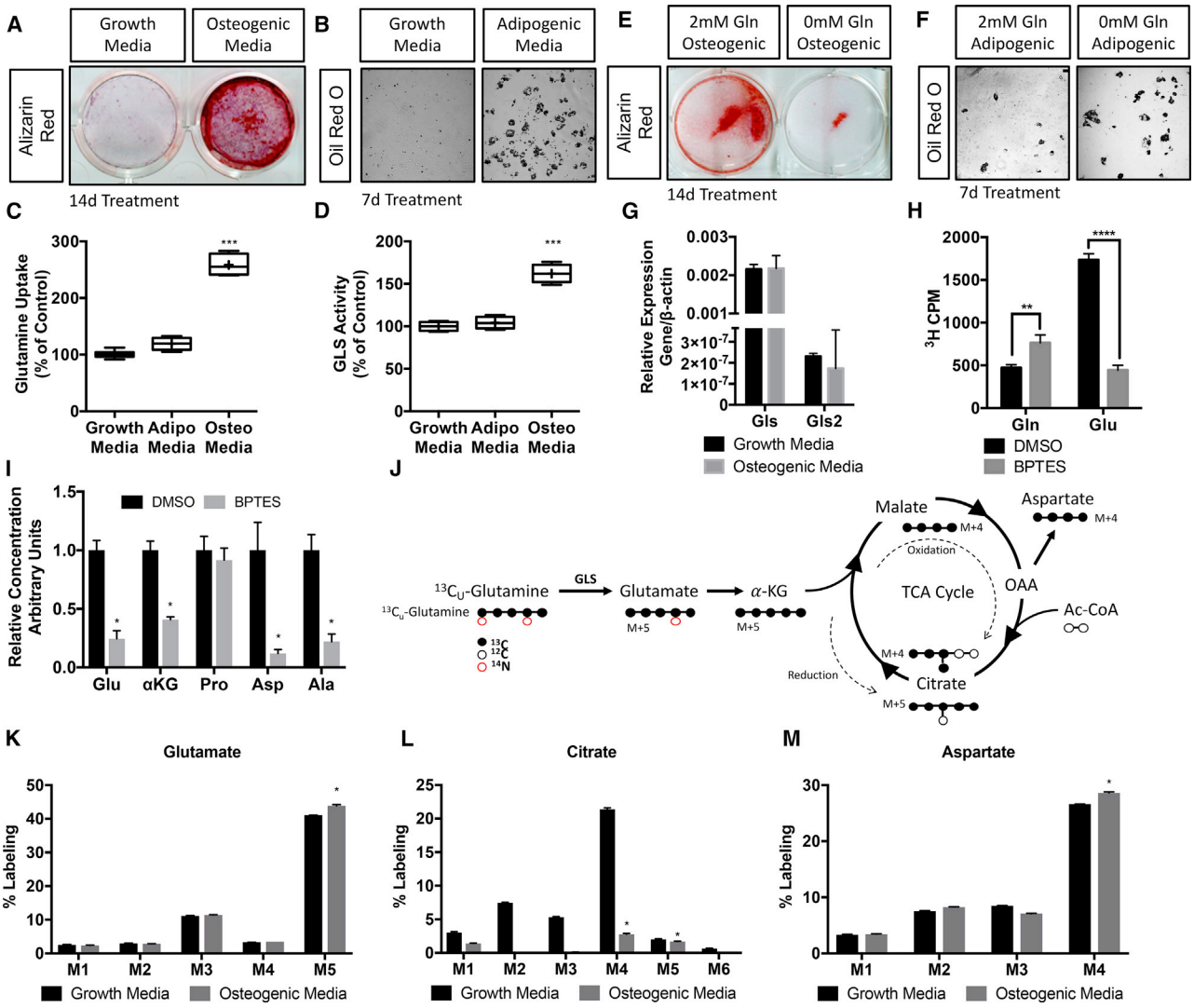

Figure 1. Skeletal Stem Cells Increase Glutamine Consumption and Metabolism during Osteoblast Differentiation

(A) Alizarin Red staining of SSCs induced to undergo osteoblast differentiation for 14 days.

(B) Oil Red O staining of SSCs induced to undergo adipocyte differentiation for 7 days.

(C and D) Tukey box and whisker plot of measurements of glutamine uptake (C) or GLS activity (D) in SSCs after 7 days of differentiation. Median and mean are represented by the line and cross, respectively. n = 5.

(E and F) Effect of glutamine withdrawal on osteoblast (E) or adipocyte (F) differentiation in SSCs.

(G) qRT-PCR analyses of gene expression in SSCs cultured for 7 days in osteogenic media.

(H) Effect of BPTES on GLS activity in SSCs.

(I) Effect of BPTES on metabolite concentration measured by mass spectrometry.

(J) Graphical depiction of tracing glutamine metabolism using [U-^{13}C]glutamine. Black filled circles indicate ^{13}C, whereas black open circles and red open circles denote ^{12}C and ^{14}N, respectively. OAA, oxaloacetate; αKG, α-ketoglutarate; ac-CoA, acetyl-CoA.

(K and M) Fractional contribution of [U-^{13}C]glutamine to glutamate (K), citrate (L), and aspartate (M). Error bars in (G)–(I) and (K)–(M) depict SD. **p ≤ 0.005, ***p ≤ 0.0005, ****p ≤ 0.00005.

See also Figure S1.

(BV/TV), trabecular number (Tb.N), and bone mineral density (BMD), while increasing trabecular separation (Tb.Sp) in both males and females at 4 months of age (Figures 2A and 2B; Table S1). *Gls* deletion also affected cortical bone, highlighted by decreased cortical thickness (Ct.Th) with no change in total bone area (T.Ar) (Figures 2C and 2D; Table S1). Histological analyses confirmed a significant reduction in trabecular bone underneath the growth plate (Figures 2E and 2F). These analyses highlighted a partially penetrant sex-dependent increase in marrow adiposity evident in 75% of *Prx1Cre;Gls$^{fl/fl}$* female mice compared to wild-type littermates at this time point (Figures 2E and 2F; p = 0.0022, binomial test). OsO_4-enhanced μCT analyses confirmed the presence of increased adiposity in the distal femurs of *Prx1Cre;Gls$^{fl/fl}$* female mice (Figures 2G and S2G). Because adipocytes and osteoblasts share a common progenitor, we next evaluated if *Gls* ablation affected osteoblast

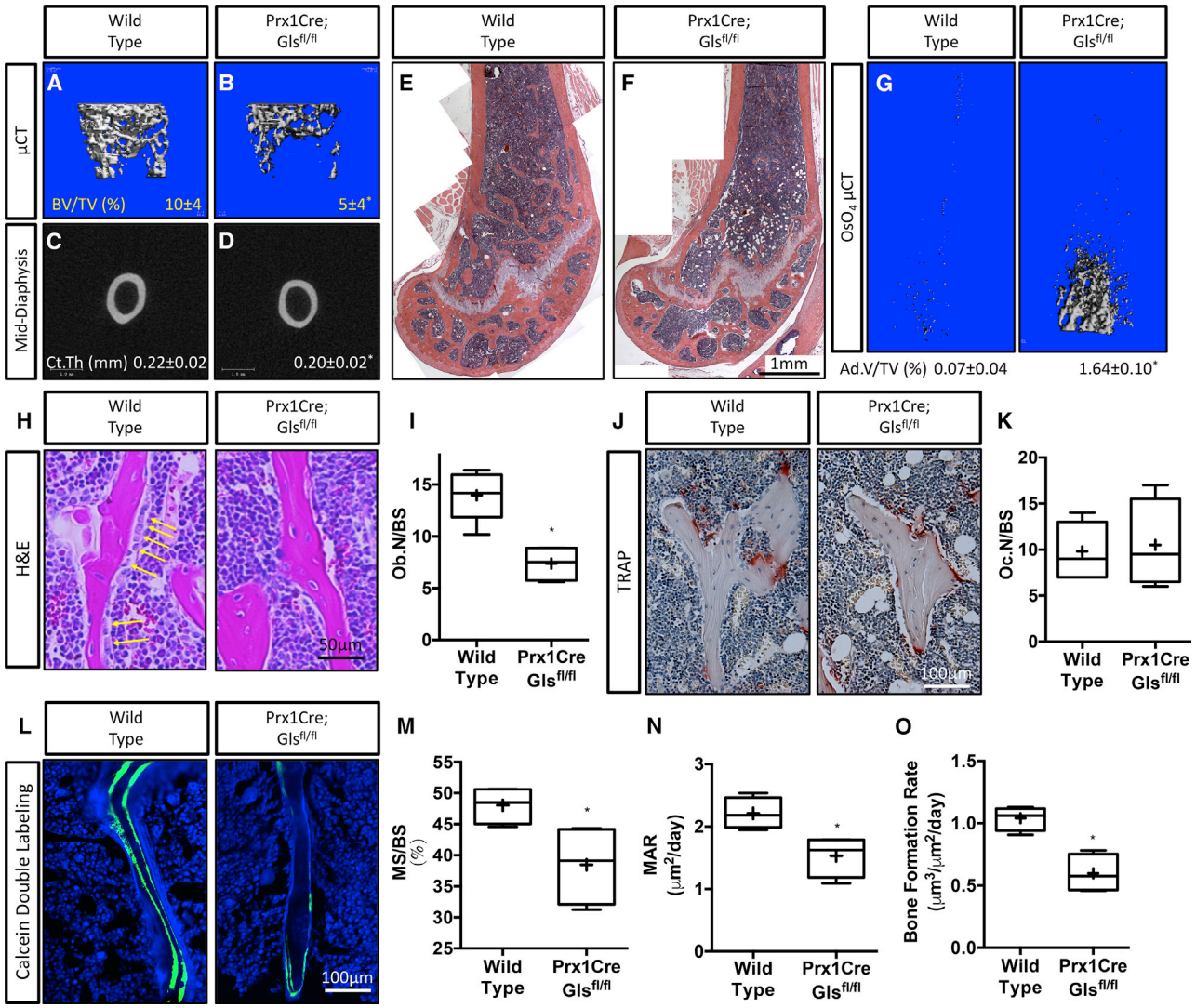

Figure 2. *Gls* Ablation Reduces Bone Mass *In Vivo*

(A–D) Representative μCT images of a 4-month-old *Prx1Cre;Gls*$^{fl/+}$ (wild-type) or *Prx1Cre;Gls*$^{fl/fl}$ mutant mouse. BV, bone volume; TV, tissue volume; Ct.Th, cortical thickness.

(E and F) Representative H&E-stained distal femur of 4-month-old female mice.

(G) Representative OsO_4 μCT images of a 4-month-old female mice. Ad.V, adipose volume; TV, tissue volume.

(H) Representative H&E-stained section used to quantify osteoblasts (arrows).

(I) Tukey box and whisker plot of the quantification of osteoblast numbers (Ob.N) per bone surface.

(J) Representative TRAP-stained section used to quantify osteoclast numbers.

(K) Tukey box and whisker plot of the quantification of osteoclast numbers (Oc.N) per bone surface.

(L) Representative calcein double labeled sections of the distal femur from 4-month-old mice.

(M–O) Tukey box and whisker plots of the quantification of mineralized surface per bone surface (MS/BS) (M), mineral apposition rate (MAR) (N), or bone formation rate (BFR) (O) derived from calcein double labeling. Median and mean are represented by the line and cross, respectively. n = 5. *p ≤ 0.05.

See also Figure S2 and Table S1.

endowment using static histomorphometry (Figures 2H and 2I). Quantification of the histomorphometric data identified a significant reduction in the overall number of osteoblasts per bone surface (Ob.N/BS) in both males and females (Figures 2H and 2I). Similarly, we observed a significant reduction in osteoblast-specific gene and protein expression in bone extracts from *Prx1Cre;Gls*$^{fl/fl}$ mice (Figures S2H and S2I). Importantly, *Gls* deletion did not affect bone resorption as we observed no change in TRAP-stained osteoclasts per bone surface (Figures 2J and 2K). We next used dynamic histomorphometry to evaluate bone formation directly (Figures 2L–2O). *Prx1Cre;Gls*$^{fl/fl}$ mice have a significant reduction in osteoblast coverage as exemplified by the mineralized surface per bone surface (MS/BS) (Figure 2M). Not only were there fewer osteoblasts in *Prx1Cre;Gls*$^{fl/fl}$ mice, but they displayed less bone-forming activity as both the mineral apposition rate (Korangath et al., 2015) and bone formation

rate (BFR) were significantly decreased in *Prx1Cre;Gls*$^{fl/fl}$ mice relative to littermate controls (Figures 2N and 2O). Thus, *Gls*-dependent glutamine metabolism is required for normal mesenchymal lineage allocation, osteoblast endowment, and bone mass accrual *in vivo*.

Glutamine Metabolism Is Required for Appropriate Specification of SSCs

We next determined how *Gls* deletion affected osteoblast endowment. We first evaluated if *Gls* deletion affected SSC maintenance and specification by performing colony-forming efficiency (CFE) assays in 2-month-old *Prx1Cre;Gls*$^{fl/+}$ (wild-type) and *Prx1Cre;Gls*$^{fl/fl}$ mice. *Prx1Cre;Gls*$^{fl/fl}$ mice displayed normal CFE, indicating the SSC population of the bone marrow was normal (Figures 3A–3C). We next stained colonies for alkaline phosphatase expression (CFU-AP) to evaluate osteoblastic specification of SSCs. *Gls* deletion resulted in reduced osteoblast specification of SSCs as we observed a significant reduction in alkaline-phosphatase-positive colonies relative to overall CFE (Figures 3D–3F). To test if the change in specification was functional, we treated colonies from wild-type and *Prx1Cre;Gls*$^{fl/fl}$ mice with either osteogenic or adipogenic media for an additional 14 days and evaluated differentiation potential. There was a significant reduction in the numbers of Von Kossa-stained osteoblastic colonies (CFU-Ob) from *Prx1Cre;Gls*$^{fl/fl}$ mice (Figures 3G–3I). Conversely, colonies isolated from *Prx1Cre;Gls*$^{fl/fl}$ mice demonstrated a significant increase in adipogenic potential as shown by increased Oil Red-O staining (CFU-Ad) (Figures 3J–3L). These data indicate that *Gls* and glutamine metabolism are required for normal SSC specification and appropriate lineage allocation. To test if *Gls* ablation affects differentiation ability directly, we performed high-density SSC cultures isolated from either wild-type or *Prx1Cre;Gls*$^{fl/fl}$ littermates. SSCs isolated from *Prx1Cre;Gls*$^{fl/fl}$ mice were able to undergo osteoblast differentiation but displayed diminished matrix mineralization as well as reduced osteoblast marker gene expression (Figures S3A and S3B). GLS knockout did not affect viability in SSCs as we observed no increase in cleaved Caspase 3, suggesting the reduction in osteoblast marker gene expression and mineralization is the result of reduced osteoblast differentiation (Figure S3C). Conversely, *Prx1Cre;Gls*$^{fl/fl}$ SSCs underwent normal adipogenic differentiation shown by Oil Red O staining and marker gene expression (Figures S3D and S3E). Unexpectedly, when cultured in media containing both adipogenic and osteogenic cues, *Prx1Cre;Gls*$^{fl/fl}$ SSCs displayed enhanced adipocyte differentiation *in vitro* with increased Oil Red O staining and adipogenic gene expression (Figures 3M and 3N). Conversely, wild-type SSCs preferentially differentiated into osteoblasts (Figures 3M and 3N). Thus, *Gls* and glutamine metabolism are critical for lineage specification and differentiation of bone marrow SSCs.

Collectively, our data indicate *Gls* and glutamine metabolism regulate osteoblast specification, differentiation, and bone formation. Because *Prx1Cre;Gls*$^{fl/fl}$ mice lack a bone phenotype prior to 2 months of age, despite deletion of *Gls* in all osteoblast lineage cells, we hypothesized *Gls* is required directly in the SSCs. Consistent with this hypothesis, deletion of *Gls* in mature osteoblasts using *BglapCre* had no effect on either bone mass or osteoblast or osteoclast numbers at 4 months of age, suggesting *Gls* is dispensable in mature osteoblasts (Figure S4; Table S2).

To test the role of *Gls* in SSCs directly, we deleted *Gls* using the *LeprCre* deleter strain that is active in SSCs that give rise to osteoblasts postnatally (Figure S5) (Mizoguchi et al., 2014; Zhou et al., 2014). μCT analyses demonstrated that while *LeprCre;Gls*$^{fl/fl}$ mice had no bone phenotype at 2 months, they had a significant decrease in bone mass in both males and females at 4 months (Figures 4A and 4B; Table S3; data not shown). The decreased bone mass in *LeprCre;Gls*$^{fl/fl}$ mice was mainly attributed to decreased trabecular numbers and increased trabecular separation (Table S3). Decreased bone mass was not the result of increased bone resorption as we found no change in the number of TRAP-positive osteoclasts in *LeprCre;Gls*$^{fl/fl}$ mice (Figures 4C–4E). Conversely, *LeprCre;Gls*$^{fl/fl}$ mice had significantly fewer osteocalcin (OCN)-positive osteoblasts compared to wild-type littermates (Figures 4H–4J). Dynamic histomorphometry revealed a significant decrease in MS/BS, MAR, and BFR specifically in the trabecular and endosteal but not periosteal compartments of *LeprCre;Gls*$^{fl/fl}$ mice (Table S3). Importantly, we did not observe increased apoptosis in LeprCre-expressing cells or their derivatives (Figure S5E).

The bone phenotype of *LeprCre;Gls*$^{fl/fl}$ mice was reminiscent of the *Prx1Cre;Gls*$^{fl/fl}$ phenotype. We next sought to determine if there was a similar marrow adiposity phenotype in these mice. Histological analyses highlighted a partially penetrant sex-dependent increase in marrow adiposity evident in 67% of *LeprCre;Gls*$^{fl/fl}$ females compared to littermate controls at 4 months of age ($n = 7$, $p \leq 0.00001$, binomial test) (Figure S5C). OsO_4-enhanced μCT analysis confirmed the presence of increased marrow fat in tibiae isolated from *LeprCre;Gls*$^{fl/fl}$ female mice (Figures 4F, 4G, and S5D). Immunofluorescent staining for the adipocyte marker perilipin (PLIN) confirmed the presence of adipocytes in the bone marrow of *LeprCre;Gls*$^{fl/fl}$ female mice (Figures 4K and 4L). Importantly, in both wild-type and *LeprCre;Gls*$^{fl/fl}$ mice, almost all PLIN$^+$ adipocytes also expressed tdTomato (88.1% ± 16.9% versus 97.8% ± 2.6%, wild-type versus *LeprCre;Gls*$^{fl/fl}$, respectively) indicating they were derived from *LeprCre*-expressing SSCs (Figures 4K and 4L). These data suggest *Gls* and glutamine metabolism are required cell autonomously for appropriate lineage allocation and osteoblast differentiation in SSCs.

Gls Is Required for SSC Proliferation

We next evaluated the CFE of *LeprCre;Gls*$^{fl/fl}$ mice. Surprisingly, *LeprCre;Gls*$^{fl/fl}$ mice displayed a significant reduction in CFE (Figures 5A and 5B). It is important to note that although the overall number of colonies containing at least 50 cells was significantly reduced in *LeprCre;Gls*$^{fl/fl}$ mice, there was no difference in the number of colonies containing at least 10 cells (Figure 5C). Indeed, there was a significant bias toward smaller colonies with fewer cells in *LeprCre;Gls*$^{fl/fl}$ mice (Figure 5D; $p < 0.0005$, binomial test, $n \geq 213$ colonies for each genotype). To determine if *Gls* and glutamine metabolism in SSCs regulate overall SSC numbers or proliferation, we performed CFE assays on cells isolated from *C57Bl/6* mice in media containing either 2 or 0 mM glutamine. Importantly, either glutamine withdrawal or GLS inhibition significantly reduced the number of colonies containing at least 50 cells and decreased the number of cells per colony (Figures 5E–5H, S6A, and S6B). These data indicate that *Gls* ablation does not affect overall SSC numbers in the bone marrow but may

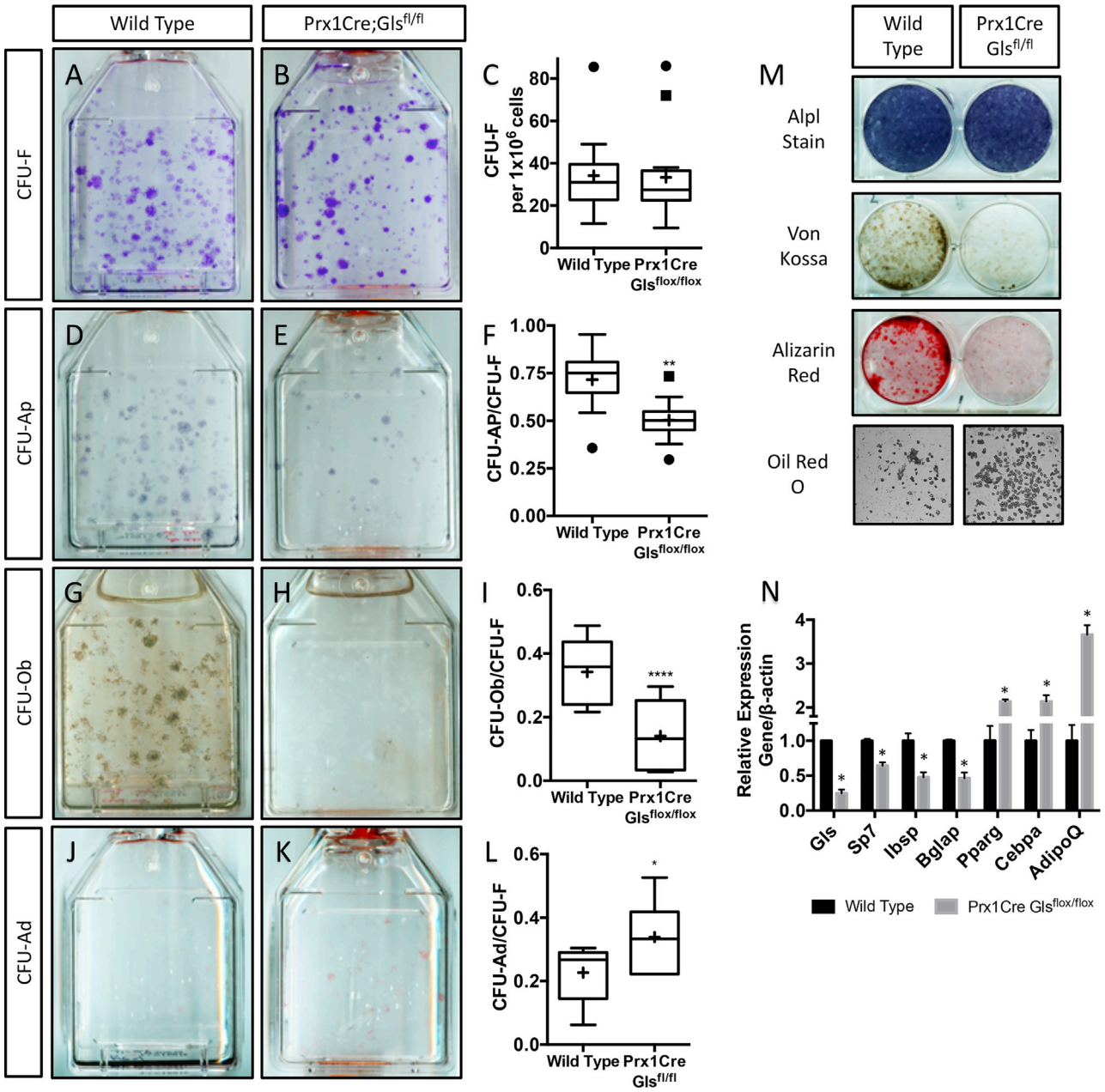

Figure 3. *Gls* Is Required for Osteoblast Specification and Differentiation from SSCs

Representative images and quantification of colony-forming unit (CFU) assays stained with Crystal Violet (A–C), alkaline phosphatase (D–F), Von Kossa (G–I), or Oil Red O (J–L).

(C, F, I, and L) Tukey box and whisker plots displaying colonies containing at least 50 cells. n = 13 or 14 for wild-type or *Prx1Cre;Gls*$^{fl/fl}$, respectively.

(M and N) Functional assays (M) or qRT-PCR analyses (N) of the effect of *Gls* deletion on cell fate decision in primary SSCs cultured in osteogenic and adipogenic media for 14 days. Error bars depict SD. n = 4 mice. *p ≤ 0.05, **p ≤ 0.005, ****p ≤ 0.00005.

See also Figure S3.

govern SSC proliferation. To test this hypothesis, we cultured SSCs isolated from *C57Bl/6* mice in the presence or absence of exogenous glutamine and evaluated proliferation. SSCs cultured without exogenous glutamine displayed a significant reduction in EDU incorporation (Figure 5I). Similarly, GLS inhibition significantly reduced both overall cell numbers and EDU incorporation in SSCs (Figures 5J and S5C–S5E). Western blot analyses demonstrate that inhibiting GLS activity significantly reduces both cyclin D1 and D3 expression (Figures 5K and 5L), indicating GLS activity is required for SSC proliferation. In support of this, we observed decreased BrdU incorporation in both Prx1Cre;Gls$^{fl/fl}$ and LeprCre;Gls$^{fl/fl}$ mice relative to wild-type

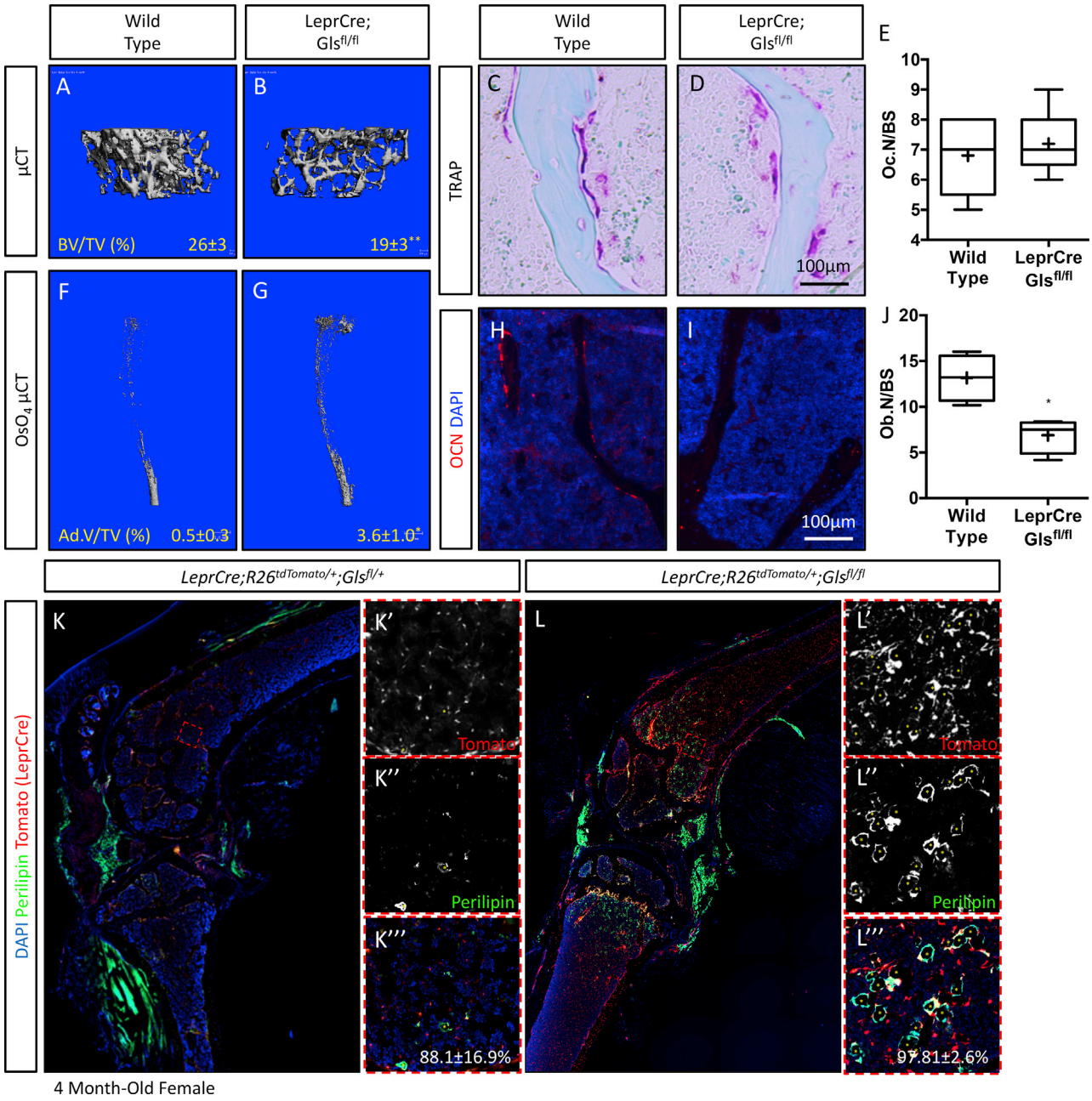

Figure 4. *Gls* Acts in SSCs to Regulate Lineage Allocation

(A and B) Representative µCT image of trabecular bone from a 4-month-old *LeprCre;Gls*$^{fl/+}$ (wild-type) or *LeprCre;Gls*$^{fl/fl}$ mutant mouse. BV, bone volume; TV, tissue volume.

(C and D) Representative TRAP-stained section used to quantify osteoclast numbers.

(E) Tukey box and whisker plot of the quantification of osteoclast numbers (Oc.N) per bone surface.

(F and G) Representative OsO_4 µCT images of the tibia from 4-month-old mice. Ad.V, adipose volume; TV, tissue volume. n = 8 or 12 for wild-type or *LeprCre;Gls*$^{fl/fl}$, respectively.

(H–J) Representative immunofluorescent staining for osteocalcin (OCN) used to quantify osteoblast numbers (Ob.N/BS) in (J).

(K) Anti-Perilipin (PLIN) and anti-tomato immunofluorescent staining of 4-month-old *LeprCre;R26*$^{tdTomato/+}$*;Gls*$^{fl/+}$ (wild-type) or *LeprCre;R26*$^{tdTomato/+}$*;Gls*$^{fl/fl}$ hindlimbs. Inset images of boxed region show individual channels (K′, K″, K‴, L′, L″, and L‴). Quantification of PLIN, tomato double-positive cells shown in (K‴ and L‴). n = 3. *p ≤ 0.05, Student's t test.

See also Figure S4 and Table S3.

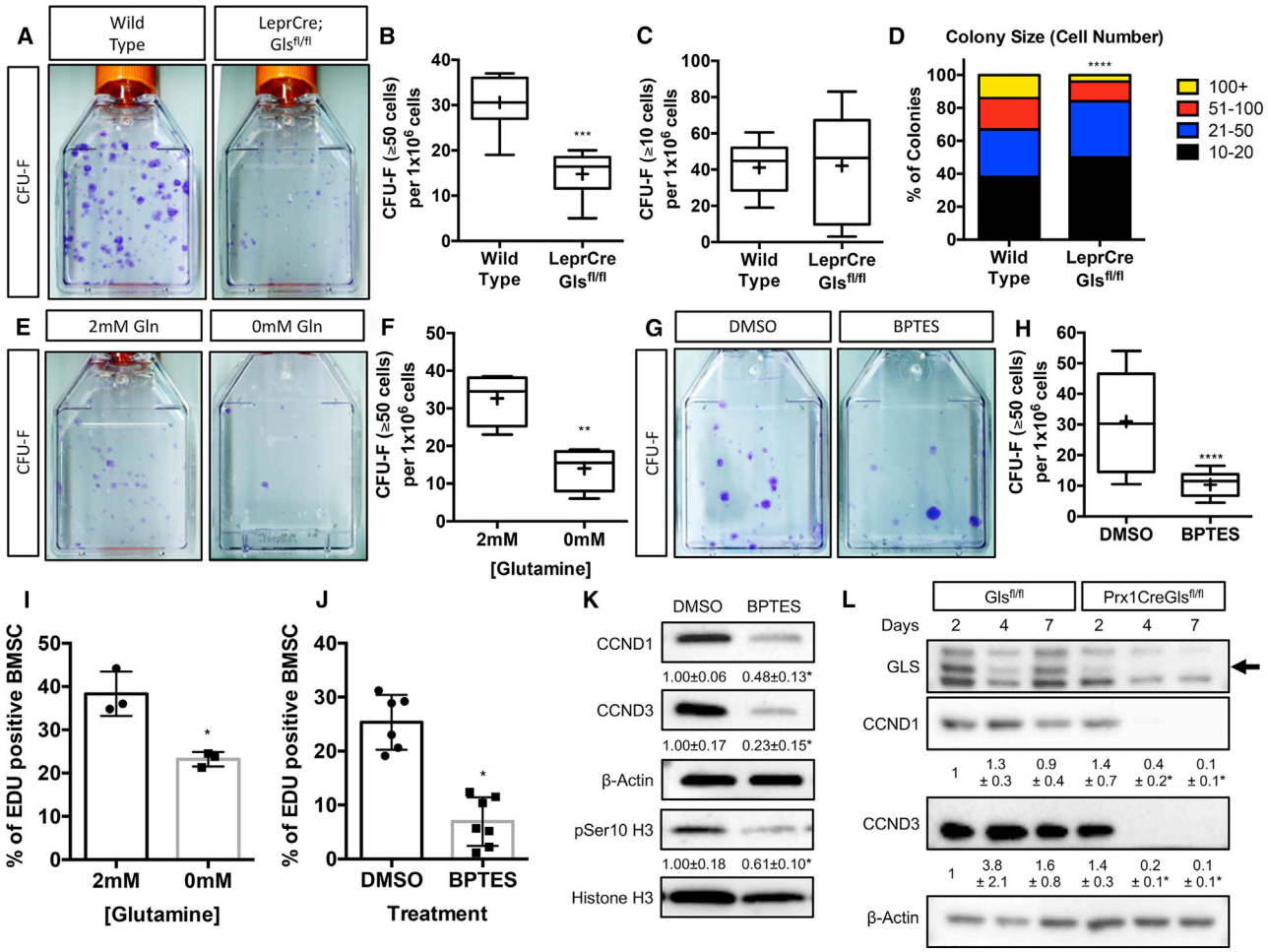

Figure 5. *Gls* Activity Is Required for SSC Proliferation and Expansion

(A) Colony-forming unit (CFU) assay of 4-month-old *LeprCre;Gls*$^{fl/+}$ (wild-type) or *LeprCre;Gls*$^{fl/fl}$ mutant littermates.

(B and C) Tukey box and whisker plots of the number of colonies per mouse containing greater than 50 cells (B) or greater than 10 cells (C).

(D) Prevalence of colonies binned for cell number. n ≥ 208 colonies from 6 animals.

(E–H) CFU assay (E and G) or Tukey box and whisker plots (F and H) showing the effect of glutamine withdrawal (E and F) or GLS inhibition treatment (G and H) on the number of colonies containing at least 50 cells isolated from 4-month-old *C57Bl/6* wild-type mice. n = 6 mice.

(I and J) Effect of glutamine withdrawal (I) or (J) GLS inhibition on EDU incorporation in SSCs. Error bars depict SD.

(K) Western blot analyses of the effect of GLS inhibition on cell cycle protein expression in ST2 cells.

(L) Western blot analyses of cell cycle markers in SSCs cultured in mineralization media for up to 7 days. Phosphorylated-histone H3 normalized to total histone H3; others normalized to β-actin. Fold change ± SD relative to control for 3 independent experiments. *p ≤ 0.05, **p ≤ 0.005, ***p ≤ 0.0005, ****p ≤ 0.00005. See also Figure S6.

controls (Figure S6F). Taken together, our data indicate GLS activity and glutamine metabolism are required for appropriate SSC proliferation.

Our metabolic analyses indicated that αKG is a primary product of glutamine metabolism in SSCs (Figure 1I). To test if glutamine derived αKG is important for colony expansion, we performed rescue experiments. αKG supplementation, but not other metabolites (e.g., nucleotides or GSH), rescued colony expansion in the absence of exogenous glutamine (Figures 6A and 6B). We next sought to understand how SSCs generate αKG from glutamine. The amino acid transaminases utilize the α nitrogen from glutamate for the biosynthesis of amino acids such as aspartate and alanine, whereas glutamate dehydrogenase deaminates glutamate to form ammonia. To determine if the transaminases are active in SSCs, we incubated SSCs with a glutamine tracer labeled with ^{15}N on the α nitrogen ($^{15}N_{\alpha}$-glutamine) for 1 h, and the contribution of the tracer to glutamate, aspartate, and alanine was determined by measuring the mass isotopolog-labeling pattern (Figure 6C). The glutamine α nitrogen is highly enriched in glutamate (M+1) as well as in both aspartate (M+1) and alanine (M+1), suggesting SSCs have high amino acid transaminase activity (Figure 6D). Importantly, GLS inhibition prevented glutamine-derived nitrogen contribution to glutamate, aspartate, or alanine (Figure 6D). Functionally, inhibiting amino acid transaminase activity using the drug AOA significantly reduced colony formation similar to GLS inhibition (Figures 6E

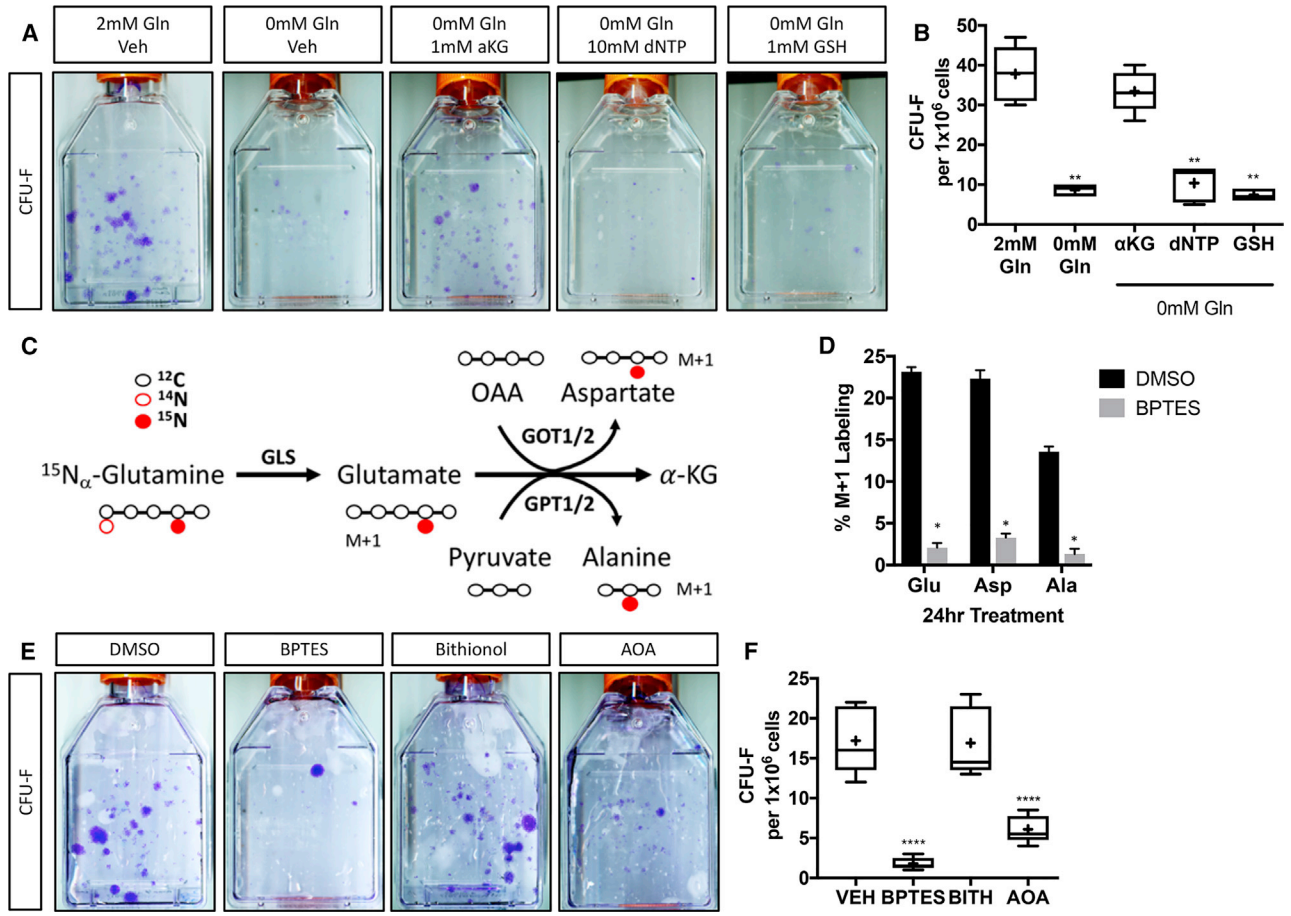

Figure 6. Transaminase-Dependent αKG Production Is Critical for SSC Proliferation

(A and B) CFU assay (A) or Tukey box and whisker plots (B) showing the effect of glutamine withdrawal and supplementation with downstream metabolites on colony formation in 4-month-old *C57Bl/6* wild-type mice. n = 5 mice.

(C) Graphical depiction of tracing glutamine metabolism using $^{15}N_{\alpha}$-glutamine. Red filled circles denote ^{15}N, whereas black and red open circles denote ^{12}C and ^{14}N, respectively. OAA, oxaloacetate.

(D) The effect of BPTES treatment on the fractional contribution of $^{15}N_{\alpha}$-glutamine to glutamate, aspartate, and alanine. Error bars depict SD.

(E and F) CFU assay (E) or Tukey box and whisker plots (F) showing the effect of BPTES, AOA, or bithionol on colony formation. n = 5 mice.

and 6F) (Korangath et al., 2015; Kauppinen et al., 1987). Conversely, glutamate dehydrogenase inhibition using bithionol had no effect on colony formation (Figures 6E and 6F) (Li et al., 2009). Collectively, these data indicate that amino acid transaminase-dependent αKG production is critical for SSC proliferation and colony expansion.

DISCUSSION

We show here that glutamine metabolism is a critical regulator of SSC proliferation, lineage allocation, and osteoblast differentiation. SSCs consume and metabolize a significant amount of glutamine as they undergo differentiation into the osteoblast but not adipocyte lineage. Genetically inhibiting glutamine metabolism in SSCs results in decreasing bone mass with age, a hallmark of age-associated osteoporosis. Mechanistically, decreased bone mass is the result of multiple factors: first, a reduction in overall osteoblast numbers. This is likely the result of decreased proliferation and altered lineage allocation favoring the adipocyte lineage in *Gls*-deficient SSCs. Second, GLS-deficient osteoblasts have reduced bone formation. Collectively, these data provide the first example of the critical role of glutamine metabolism in SSCs to regulate lineage allocation and bone homeostasis in mice.

SSCs give rise to both osteoblasts and adipocytes throughout life. Interestingly, bone mass and marrow adiposity are known to be negatively correlated. The loss of *Gls* in SSCs resulted in decreased bone mass in both males and females and increased marrow adiposity apparent only in female mice. It is unclear from these experiments if males have a similar adiposity phenotype as we only evaluated mice at 4 months of age; thus, it is possible male mice at older time points also have increased adiposity. However, marrow adiposity, much like bone mass, is a sexually dimorphic trait. Female mice have lower bone mass and are reported to have over ten times more marrow adipocytes in the proximal tibia relative to male mice (Lecka-Czernik et al., 2017). Thus, it is plausible that extrinsic factors disparately influence marrow adiposity in male and female mice. Importantly,

SSCs from male *Gls* knockout mice were more receptive to adipogenic cues *in vitro*—supporting an intrinsic role for glutamine metabolism in lineage specification (Figure 3). Future studies are needed to understand this phenomenon.

SSCs metabolize glutamine to support both proliferation and osteoblast specification. Glutamine has long been recognized as an important nutrient in proliferating cells in culture (Eagle et al., 1956; Eagle, 1955). Glutamine is essential to progress through the G1 restriction point as well as exit S phase to begin cell division (Colombo et al., 2011). Consistent with these data, inhibition of GLS in SSCs reduced the expression of cell markers cyclin D1 and D3 as well as EDU incorporation (Figures 5I–5L). This is consistent with a recent report demonstrating glutamine metabolism is required to support endothelial cell proliferation *in vivo* (Huang et al., 2017; Kim et al., 2017). Our data demonstrate that amino-acid-transaminase-derived αKG is the critical downstream metabolite regulating proliferation in SSCs (Figures 1I and 6). Aspartate biosynthesis was reported to be critical for proliferation by providing carbon and nitrogen for synthetic reactions necessary for proliferation (Birsoy et al., 2015; Sullivan et al., 2015). Future studies are warranted to determine if glutamine-dependent aspartate biosynthesis contributes to proliferation in SSCs.

During our CFU analyses comparing the *Prx1Cre;Gls*$^{fl/fl}$ and *LeprCre;Gls*$^{fl/fl}$ mice, we uncovered an apparent disparity in the CFE between mutant genotypes. One would predict that the CFE would be similar between these mutant genotypes; however, *LeprCre;Gls*$^{fl/fl}$ mutants exhibit fewer CFU-F while *Prx1Cre;Gls*$^{fl/fl}$ mutants show no significant difference compared to controls. There are two possible explanations for this. First, based on the expression of both *Prx1Cre* and *LeprCre* (Figures S2 and S4), *Gls* deletion using *LeprCre* might place *Gls* null SSCs at a competitive disadvantage relative to surrounding wild-type cells able to utilize glutamine to support proliferation (Zhou et al., 2014; Logan et al., 2002). By comparison, *Prx1Cre* is more broadly expressed in the bone marrow, resulting in less of a competitive disadvantage for *Gls* null SSCs and minimal effect on proliferation. Second, SSCs may be addicted to glutamine metabolism to support proliferation similar to some cancer cells (Wise and Thompson, 2010). However, if SSCs are derived from cells unable to metabolize glutamine, they avoid the glutamine addiction and can proliferate and function normally. *Prx1Cre* is active beginning at embryonic day 9.5 in cells that give rise to the SSC population, whereas *LeprCre* is not active until the SSC forms (Greenbaum et al., 2013; Logan et al., 2002). In this scenario, *Prx1Cre;Gls*$^{fl/fl}$ SSCs have never been able to metabolize glutamine and have overcome this deficiency, whereas *LeprCre;Gls*$^{fl/fl}$ SSC are unable to overcome the acute loss of glutamine metabolism. Our data support this hypothesis, as glutamine withdrawal and GLS inhibition both phenocopied the *LeprCre;Gls*$^{fl/fl}$ CFE phenotype despite inhibiting glutamine metabolism in all plated cells (Figures 5A–5G). It is important to note *Prx1Cre;Gls*$^{fl/fl}$ SSCs had diminished proliferation when induced to undergo osteoblast differentiation, suggesting they are unable to compensate for the loss of glutamine metabolism in certain instances (Figure 5L).

Cellular metabolism is emerging as a critical regulator of stem cell maintenance, cell fate determination, and differentiation in various contexts (Oburoglu et al., 2014; Knobloch et al., 2013; Ito et al., 2012). For example, alterations in glucose metabolism promote osteoblast fate at the expense of adipocyte fate through epigenetic regulation of gene expression (Karner et al., 2016). Similarly, our data indicate glutamine metabolism is required for appropriate lineage allocation in SSCs. The precise mechanism by which glutamine metabolism acts is unknown. Lineage commitment and differentiation likely present SSCs with diverse energetic, biosynthetic, and antioxidant demands. For example, osteoblasts increase protein synthesis and secretion during differentiation, both energetically demanding processes. Conversely, adipocytes are known to store energy in the form of lipids. In SSCs, glutamine does not appear to be a major energetic substrate as glutamine contribution to citrate declined during osteoblast differentiation, and GLS inhibition did not induce energetic stress (Figures 1L and S1K). We postulate glycolysis offsets this as recent reports indicate that glycolysis increases during osteoblast differentiation and that osteoblasts derive most of their ATP from glycolysis (Guntur et al., 2014; Komarova et al., 2000; Borle et al., 1960). Metabolic flexibility is likely important to allow SSCs to best utilize available nutrients to respond to diverse cellular demands associated with proliferation, specification, and differentiation. In contrast to energetics, glutamine contribution to GSH increased during osteoblast differentiation (Figure S1K). This may be important to offset reactive oxygen species (ROS) known to be detrimental to the osteoblast fate (Wang et al., 2015; Tormos et al., 2011; Chen et al., 2008; Almeida et al., 2007; Bai et al., 2004; Mody et al., 2001). In the case of adipocyte differentiation, glutamine may be less important given the positive role of ROS (Wang et al., 2015; Tormos et al., 2011).

Osteoblasts are known to express an array of SIBLING (e.g., osteopontin), GLA (e.g., osteocalcin), and acidic glycoproteins (e.g., osteonectin and sialoprotein II) that function to regulate collagen mineralization. These proteins are significantly enriched for both aspartate and glutamate residues. Glutamine metabolism is critical to maintain levels of both glutamate and aspartate in SSCs as glutamine contributes both carbon and nitrogen for glutamate and aspartate biosynthesis. It is intriguing to speculate that glutamine metabolism fulfills this unique synthetic requirement of osteoblasts and thus promotes collagen mineralization and bone formation. Another possibility is that glutamine metabolism epigenetically regulates lineage allocation in SSCs. αKG is a cofactor for both Jumonji-domain-containing histone demethylases and the TET family of DNA demethylases (McDonough et al., 2010; Schofield and Zhang, 1999). A reduction in glutamine-derived αKG is predicted to reduce DNA and histone demethylation—potentially biasing lineage commitment. Indeed, Tet1 and Tet2 are necessary for SSC self-renewal and osteoblast differentiation (Yang et al., 2018). Our data demonstrate GLS, and thus glutamine, is at the apex of a complex regulatory network in SSCs. Future studies will be necessary to elucidate the precise mechanisms by which glutamine metabolism impacts SSCs through the epigenetic regulation of osteogenic factors, the generation of amino acids critically important to specific osteoblast and bone-forming proteins, and the regulation of ROS.

Limitations of Study

In summary, while our study demonstrates the critical role of GLS and glutamine metabolism in the regulation of SSC proliferation

and osteoblast endowment, the precise molecular details remain to be resolved. Our data highlight αKG as a critical regulator of SSC proliferation; however, the mechanism by which αKG regulates proliferation is unclear. Similarly, the roles of αKG during lineage allocation and osteoblast differentiation remain to be elucidated. It is important to note our data do not exclude the possibility that multiple downstream metabolites are required for osteoblast specification and differentiation in SSCs. Regardless, our data highlight a previously unknown role for glutamine metabolism in regulating bone homeostasis.

STAR★METHODS

Detailed methods are provided in the online version of this paper and include the following:

- KEY RESOURCES TABLE
- CONTACT FOR REAGENT AND RESOURCE SHARING
- EXPERIMENTAL MODEL AND SUBJECT DETAILS
  - Mouse Strains
  - Primary Cells and Cell Lines
- METHOD DETAILS
  - Mouse Analyses
  - Cell Culture
  - Mass Spectrometry Analysis of Glutamine Metabolism
  - GSH and GSSG Labeling Analysis by LC-MS/MS
  - Glutaminase Activity Assay
  - RNA Isolation and qPCR
  - Western Blotting
- QUANTIFICATION AND STATISTICAL ANALYSIS

SUPPLEMENTAL INFORMATION

Supplemental Information includes six figures and four tables and can be found with this article online at https://doi.org/10.1016/j.cmet.2019.01.016.

ACKNOWLEDGMENTS

The authors thank Drs. Thomas Carroll and Ryan Gray for critical comments on this manuscript. This work was supported by NIH R01 grants 2AR063071 to M.J.H. and AR071967 to C.M.K.

AUTHOR CONTRIBUTIONS

Conceptualization, C.M.K.; Investigation, Y.Y., H.N., L.S., D.S., G.H., A.J.M., H.Z., E.K., G.-F.Z., M.J.H., and C.M.K.; Writing – Original Draft, C.M.K.; Writing – Review & Editing, G.-F.Z., M.J.H., and C.M.K.; Supervision, C.M.K.

DECLARATION OF INTERESTS

The authors declare no competing interests.

Received: February 1, 2018
Revised: November 15, 2018
Accepted: January 20, 2019
Published: February 14, 2019

REFERENCES

Almeida, M., Han, L., Martin-Millan, M., O'Brien, C.A., and Manolagas, S.C. (2007). Oxidative stress antagonizes Wnt signaling in osteoblast precursors by diverting beta-catenin from T cell factor- to forkhead box O-mediated transcription. J. Biol. Chem. *282*, 27298–27305.

Bai, X.C., Lu, D., Bai, J., Zheng, H., Ke, Z.Y., Li, X.M., and Luo, S.Q. (2004). Oxidative stress inhibits osteoblastic differentiation of bone cells by ERK and NF-kappaB. Biochem. Biophys. Res. Commun *314*, 197–207.

Balani, D.H., Ono, N., and Kronenberg, H.M. (2017). Parathyroid hormone regulates fates of murine osteoblast precursors in vivo. J.Clin. Invest *127*, 3327–3338.

Becker, D.J., Kilgore, M.L., and Morrisey, M.A. (2010). The societal burden of osteoporosis. Curr. Rheumatol. Rep *12*, 186–191.

Bianco, P., and Robey, P.G. (2015). Skeletal stem cells. Development *142*, 1023–1027.

Birsoy, K., Wang, T., Chen, W.W., Freinkman, E., Abu-Remaileh, M., and Sabatini, D.M. (2015). An essential role of the mitochondrial electron transport chain in cell proliferation is to enable aspartate synthesis. Cell *162*, 540–551.

Borle, A.B., Nichols, N., and Nichols, G., Jr. (1960). Metabolic studies of bone in vitro. I. Normal bone. J. Biol. Chem. *235*, 1206–1210.

Chen, C.T., Shih, Y.R., Kuo, T.K., Lee, O.K., and Wei, Y.H. (2008). Coordinated changes of mitochondrial biogenesis and antioxidant enzymes during osteogenic differentiation of human mesenchymal stem cells. Stem Cells *26*, 960–968.

Colombo, S.L., Palacios-Callender, M., Frakich, N., Carcamo, S., Kovacs, I., Tudzarova, S., and Moncada, S. (2011). Molecular basis for the differential use of glucose and glutamine in cell proliferation as revealed by synchronized HeLa cells. Proc. Natl. Acad. Sci. USA *108*, 21069–21074.

D'Ippolito, G., Schiller, P.C., Ricordi, C., Roos, B.A., and Howard, G.A. (1999). Age-related osteogenic potential of mesenchymal stromal stem cells from human vertebral bone marrow. J. Bone Miner. Res. *14*, 1115–1122.

DeBerardinis, R.J., Mancuso, A., Daikhin, E., Nissim, I., Yudkoff, M., Wehrli, S., and Thompson, C.B. (2007). Beyond aerobic glycolysis: transformed cells can engage in glutamine metabolism that exceeds the requirement for protein and nucleotide synthesis. Proc. Natl. Acad. Sci. USA *104*, 19345–19350.

DeFalco, J., Tomishima, M., Liu, H., Zhao, C., Cai, X., Marth, J.D., Enquist, L., and Friedman, J.M. (2001). Virus-assisted mapping of neural inputs to a feeding center in the hypothalamus. Science *291*, 2608–2613.

Ding, L., and Morrison, S.J. (2013). Haematopoietic stem cells and early lymphoid progenitors occupy distinct bone marrow niches. Nature *495*, 231–235.

Eagle, H. (1955). Nutrition needs of mammalian cells in tissue culture. Science *122*, 501–514.

Eagle, H., Oyama, V.I., Levy, M., Horton, C.L., and Fleischman, R. (1956). The growth response of mammalian cells in tissue culture to L-glutamine and L-glutamic acid. J. Biol. Chem. *218*, 607–616.

Egan, K.P., Brennan, T.A., and Pignolo, R.J. (2012). Bone histomorphometry using free and commonly available software. Histopathology *61*, 1168–1173.

Eisman, J.A., Bogoch, E.R., Dell, R., Harrington, J.T., McKinney, R.E., Jr., McLellan, A., Mitchell, P.J., Silverman, S., Singleton, R., Siris, E., et al. (2012). Making the first fracture the last fracture: ASBMR task force report on secondary fracture prevention. J. Bone Miner. Res. *27*, 2039–2046.

Fairfield, H., Falank, C., Harris, E., Demambro, V., McDonald, M., Pettitt, J.A., Mohanty, S.T., Croucher, P., Kramer, I., Kneissel, M., et al. (2018). The skeletal cell-derived molecule sclerostin drives bone marrow adipogenesis. J. Cell. Physiol *233*, 1156–1167.

Fan, Y., Hanai, J.I., Le, P.T., Bi, R., Maridas, D., DeMambro, V., Figueroa, C.A., Kir, S., Zhou, X., Mannstadt, M., et al. (2017). Parathyroid hormone directs bone marrow mesenchymal cell fate. Cell Metab *25*, 661–672.

Friedenstein, A.J., Piatetzky, S., II, and Petrakova, K.V. (1966). Osteogenesis in transplants of bone marrow cells. J. Embryol. Exp. Morphol *16*, 381–390.

Greenbaum, A., Hsu, Y.M., Day, R.B., Schuettpelz, L.G., Christopher, M.J., Borgerding, J.N., Nagasawa, T., and Link, D.C. (2013). CXCL12 in early mesenchymal progenitors is required for haematopoietic stem-cell maintenance. Nature *495*, 227–230.

Guntur, A.R., Le, P.T., Farber, C.R., and Rosen, C.J. (2014). Bioenergetics during calvarial osteoblast differentiation reflect strain differences in bone mass. Endocrinology *155*, 1589–1595.

Huang, H., Vandekeere, S., Kalucka, J., Bierhansl, L., Zecchin, A., Bruning, U., Visnagri, A., Yuldasheva, N., Goveia, J., Cruys, B., et al. (2017). Role of glutamine and interlinked asparagine metabolism in vessel formation. EMBO J *36*, 2334–2352.

Ito, K., Carracedo, A., Weiss, D., Arai, F., Ala, U., Avigan, D.E., Schafer, Z.T., Evans, R.M., Suda, T., Lee, C.H., et al. (2012). A PML-PPAR-delta pathway for fatty acid oxidation regulates hematopoietic stem cell maintenance. Nat. Med *18*, 1350–1358.

Justesen, J., Stenderup, K., Ebbesen, E.N., Mosekilde, L., Steiniche, T., and Kassem, M. (2001). Adipocyte tissue volume in bone marrow is increased with aging and in patients with osteoporosis. Biogerontology *2*, 165–171.

Karner, C.M., Esen, E., Okunade, A.L., Patterson, B.W., and Long, F. (2015). Increased glutamine catabolism mediates bone anabolism in response to WNT signaling. J. Clin. Invest *125*, 551–562.

Karner, C.M., Esen, E., Chen, J., Hsu, F.F., Turk, J., and Long, F. (2016). Wnt protein signaling reduces nuclear acetyl-coa levels to suppress gene expression during osteoblast differentiation. J. Biol. Chem. *291*, 13028–13039.

Kauppinen, R.A., Sihra, T.S., and Nicholls, D.G. (1987). Aminooxyacetic acid inhibits the malate-aspartate shuttle in isolated nerve terminals and prevents the mitochondria from utilizing glycolytic substrates. Biochim. Biophys. Acta *930*, 173–178.

Kim, B., Li, J., Jang, C., and Arany, Z. (2017). Glutamine fuels proliferation but not migration of endothelial cells. EMBO J *36*, 2321–2333.

Knobloch, M., Braun, S.M., Zurkirchen, L., von Schoultz, C., Zamboni, N., Arauzo-Bravo, M.J., Kovacs, W.J., Karalay, O., Suter, U., Machado, R.A., et al. (2013). Metabolic control of adult neural stem cell activity by Fasn-dependent lipogenesis. Nature *493*, 226–230.

Komarova, S.V., Ataullakhanov, F.I., and Globus, R.K. (2000). Bioenergetics and mitochondrial transmembrane potential during differentiation of cultured osteoblasts. Am. J. Physiol. Cell Physiol. *279*, C1220–C1229.

Kombu, R.S., Zhang, G.F., Abbas, R., Mieyal, J.J., Anderson, V.E., Kelleher, J.K., Sanabria, J.R., and Brunengraber, H. (2009). Dynamics of glutathione and ophthalmate traced with 2H-enriched body water in rats and humans. Am. J. Physiol. Endocrinol. Metab. *297*, E260–E269.

Korangath, P., Teo, W.W., Sadik, H., Han, L., Mori, N., Huijts, C.M., Wildes, F., Bharti, S., Zhang, Z., Santa-Maria, C.A., et al. (2015). Targeting glutamine metabolism in breast cancer with aminooxyacetate. Clin. Cancer Res. *21*, 3263–3273.

Le, A., Lane, A.N., Hamaker, M., Bose, S., Gouw, A., Barbi, J., Tsukamoto, T., Rojas, C.J., Slusher, B.S., Zhang, H., et al. (2012). Glucose-independent glutamine metabolism via TCA cycling for proliferation and survival in B cells. Cell Metab *15*, 110–121.

Lecka-Czernik, B., Stechschulte, L.A., Czernik, P.J., Sherman, S.B., Huang, S., and Krings, A. (2017). Marrow adipose tissue: skeletal location, sexual dimorphism, and response to sex steroid deficiency. Front. Endocrinol. (Lausanne) *8*, 188.

Li, M., Smith, C.J., Walker, M.T., and Smith, T.J. (2009). Novel inhibitors complexed with glutamate dehydrogenase: allosteric regulation by control of protein dynamics. J. Biol. Chem. *284*, 22988–23000.

Li, J., Zhang, N., Huang, X., Xu, J., Fernandes, J.C., Dai, K., and Zhang, X. (2013). Dexamethasone shifts bone marrow stromal cells from osteoblasts to adipocytes by C/EBPalpha promoter methylation. Cell Death Dis *4*, e832.

Logan, M., Martin, J.F., Nagy, A., Lobe, C., Olson, E.N., and Tabin, C.J. (2002). Expression of Cre recombinase in the developing mouse limb bud driven by a Prxl enhancer. Genesis *33*, 77–80.

Masson, J., Darmon, M., Conjard, A., Chuhma, N., Ropert, N., Thoby-Brisson, M., Foutz, A.S., Parrot, S., Miller, G.M., Jorisch, R., et al. (2006). Mice lacking brain/kidney phosphate-activated glutaminase have impaired glutamatergic synaptic transmission, altered breathing, disorganized goal-directed behavior and die shortly after birth. J. Neurosci *26*, 4660–4671.

McDonough, M.A., Loenarz, C., Chowdhury, R., Clifton, I.J., and Schofield, C.J. (2010). Structural studies on human 2-oxoglutarate dependent oxygenases. Curr. Opin. Struct. Biol. *20*, 659–672.

Meister, A. (1975). Function of glutathione in kidney via the gamma-glutamyl cycle. Med. Clin. North. Am. *59*, 649–666.

Metallo, C.M., Gameiro, P.A., Bell, E.L., Mattaini, K.R., Yang, J., Hiller, K., Jewell, C.M., Johnson, Z.R., Irvine, D.J., Guarente, L., et al. (2011). Reductive glutamine metabolism by IDH1 mediates lipogenesis under hypoxia. Nature *481*, 380–384.

Mizoguchi, T., Pinho, S., Ahmed, J., Kunisaki, Y., Hanoun, M., Mendelson, A., Ono, N., Kronenberg, H.M., and Frenette, P.S. (2014). Osterix marks distinct waves of primitive and definitive stromal progenitors during bone marrow development. Dev. Cell *29*, 340–349.

Mody, N., Parhami, F., Sarafian, T.A., and Demer, L.L. (2001). Oxidative stress modulates osteoblastic differentiation of vascular and bone cells. Free Radic. Biol. Med *31*, 509–519.

Moerman, E.J., Teng, K., Lipschitz, D.A., and Lecka-Czernik, B. (2004). Aging activates adipogenic and suppresses osteogenic programs in mesenchymal marrow stroma/stem cells: the role of PPAR-gamma2 transcription factor and TGF-beta/BMP signaling pathways. Aging Cell *3*, 379–389.

Mullen, A.R., Wheaton, W.W., Jin, E.S., Chen, P.H., Sullivan, L.B., Cheng, T., Yang, Y., Linehan, W.M., Chandel, N.S., and DeBerardinis, R.J. (2011). Reductive carboxylation supports growth in tumour cells with defective mitochondria. Nature *481*, 385–388.

Nishida, S., Endo, N., Yamagiwa, H., Tanizawa, T., and Takahashi, H.E. (1999). Number of osteoprogenitor cells in human bone marrow markedly decreases after skeletal maturation. J. Bone Miner. Metab *17*, 171–177.

Oburoglu, L., Tardito, S., Fritz, V., de Barros, S.C., Merida, P., Craveiro, M., Mamede, J., Cretenet, G., Mongellaz, C., An, X., et al. (2014). Glucose and glutamine metabolism regulate human hematopoietic stem cell lineage specification. Cell Stem Cell *15*, 169–184.

Owen, M., and Friedenstein, A.J. (1988). Stromal stem cells: marrow-derived osteogenic precursors. Ciba Found. Symp *136*, 42–60.

Park, D., Spencer, J.A., Koh, B.I., Kobayashi, T., Fujisaki, J., Clemens, T.L., Lin, C.P., Kronenberg, H.M., and Scadden, D.T. (2012). Endogenous bone marrow MSCs are dynamic, fate-restricted participants in bone maintenance and regeneration. Cell Stem Cell *10*, 259–272.

Scheller, E.L., Troiano, N., Vanhoutan, J.N., Bouxsein, M.A., Fretz, J.A., Xi, Y., Nelson, T., Katz, G., Berry, R., Church, C.D., et al. (2014). Use of osmium tetroxide staining with microcomputerized tomography to visualize and quantify bone marrow adipose tissue in vivo. Methods Enzymol *537*, 123–139.

Schofield, C.J., and Zhang, Z. (1999). Structural and mechanistic studies on 2-oxoglutarate-dependent oxygenases and related enzymes. Curr. Opin. Struct. Biol. *9*, 722–731.

Stein, W.H., and Moore, S. (1954). The free amino acids of human blood plasma. J. Biol. Chem. *211*, 915–926.

Still, E.R., and Yuneva, M.O. (2017). Hopefully devoted to Q: targeting glutamine addiction in cancer. Br. J. Cancer *116*, 1375–1381.

Sullivan, L.B., Gui, D.Y., Hosios, A.M., Bush, L.N., Freinkman, E., and Vander Heiden, M.G. (2015). Supporting aspartate biosynthesis is an essential function of respiration in proliferating cells. Cell *162*, 552–563.

Thangavelu, K., Pan, C.Q., Karlberg, T., Balaji, G., Uttamchandani, M., Suresh, V., Schuler, H., Low, B.C., and Sivaraman, J. (2012). Structural basis for the allosteric inhibitory mechanism of human kidney-type glutaminase (KGA) and its regulation by Raf-Mek-Erk signaling in cancer cell metabolism. Proc. Natl. Acad. Sci. USA *109*, 7705–7710.

Tormos, K.V., Anso, E., Hamanaka, R.B., Eisenbart, J., Joseph, J., Kalyanaraman, B., and Chandel, N.S. (2011). Mitochondrial complex III ROS regulate adipocyte differentiation. Cell Metab *14*, 537–544.

U.S. Department of Health and Human Services (2004). Bone Health and Osteoporosis: A Report of the Surgeon General (Rockville, MD: U.S. Department of Health and Human Services, Office of the Surgeon General).

Velletri, T., Romeo, F., Tucci, P., Peschiaroli, A., Annicchiarico-Petruzzelli, M., Niklison-Chirou, M.V., Amelio, I., Knight, R.A., Mak, T.W., Melino, G., et al. (2013). GLS2 is transcriptionally regulated by p73 and contributes to neuronal differentiation. Cell Cycle *12*, 3564–3573.

Wang, W., Zhang, Y., Lu, W., and Liu, K. (2015). Mitochondrial reactive oxygen species regulate adipocyte differentiation of mesenchymal stem cells in hematopoietic stress induced by arabinosylcytosine. PLoS One *10*, e0120629.

Wang, Y., Christopher, B.A., Wilson, K.A., Muoio, D., McGarrah, R.W., Brunengraber, H., and Zhang, G.F. (2018). Propionate-induced changes in cardiac metabolism, notably CoA trapping, are not altered by l-carnitine. Am. J. Physiol. Endocrinol. Metab. *315*, E622–E633.

Wise, D.R., and Thompson, C.B. (2010). Glutamine addiction: a new therapeutic target in cancer. Trends Biochem. Sci. *35*, 427–433.

Wise, D.R., Ward, P.S., Shay, J.E., Cross, J.R., Gruber, J.J., Sachdeva, U.M., Platt, J.M., DeMatteo, R.G., Simon, M.C., and Thompson, C.B. (2011). Hypoxia promotes isocitrate dehydrogenase-dependent carboxylation of alpha-ketoglutarate to citrate to support cell growth and viability. Proc. Natl. Acad. Sci. USA *108*, 19611–19616.

Wu, M., Wang, Y., Shao, J.Z., Wang, J., Chen, W., and Li, Y.P. (2017). Cbfbeta governs osteoblast-adipocyte lineage commitment through enhancing beta-catenin signaling and suppressing adipogenesis gene expression. Proc. Natl. Acad. Sci. USA *114*, 10119–10124.

Yang, R., Yu, T., Kou, X., Gao, X., Chen, C., Liu, D., Zhou, Y., and Shi, S. (2018). Tet1 and Tet2 maintain mesenchymal stem cell homeostasis via demethylation of the P2rX7 promoter. Nat. Commun *9*, 2143.

Yue, R., Zhou, B.O., Shimada, I.S., Zhao, Z., and Morrison, S.J. (2016). Leptin receptor promotes adipogenesis and reduces osteogenesis by regulating mesenchymal stromal cells in adult bone marrow. Cell Stem Cell *18*, 782–796.

Zhang, M., Xuan, S., Bouxsein, M.L., von Stechow, D., Akeno, N., Faugere, M.C., Malluche, H., Zhao, G., Rosen, C.J., Efstratiadis, A., et al. (2002). Osteoblast-specific knockout of the insulin-like growth factor (IGF) receptor gene reveals an essential role of IGF signaling in bone matrix mineralization. J. Biol. Chem. *277*, 44005–44012.

Zhang, J., Pavlova, N.N., and Thompson, C.B. (2017). Cancer cell metabolism: the essential role of the nonessential amino acid, glutamine. EMBO J *36*, 1302–1315.

Zhou, B.O., Yue, R., Murphy, M.M., Peyer, J.G., and Morrison, S.J. (2014). Leptin-receptor-expressing mesenchymal stromal cells represent the main source of bone formed by adult bone marrow. Cell Stem Cell. *15*, 154–168.

STAR★METHODS

KEY RESOURCES TABLE

REAGENT or RESOURCE	SOURCE	IDENTIFIER
Antibodies		
Anti-Osteocalcin	Millipore	RRID: AB_1587337
Anti-BRDU	Thermofisher	RRID: AB_10986341
Anti-Perilipin	Abcam	RRID: AB_10829911
Anti-GLS	Abcam	RRID: AB_2110382
Anti-Cyclin D1	Cell Signaling Technology	RRID: AB_2228523
Anti-Cyclin D3	Cell Signaling Technology	RRID: AB_2070801
Anti-α-tubulin	Cell Signaling Technology	RRID: AB_2210548
Anti-AMPK	Cell Signaling Technology	RRID: AB_330331
Anti-P-T172 AMPK	Cell Signaling Technology	RRID: AB_330330
Anti-Eif2α	Cell Signaling Technology	RRID: AB_10692650
Anti-P-S51 Eif2α	Cell Signaling Technology	RRID: AB_2096481
Anti-Chop	Cell Signaling Technology	RRID: AB_2089254
Anti-Atf4	Santa Cruz	RRID: AB_2058752
Anti-β-actin	Cell Signaling Technology	RRID: AB_330288
Anti-HRP goat anti-rabbit	Cell Signaling Technology	RRID: AB_2099233
Anti-HRP anti-mouse	Cell Signaling Technology	RRID: AB_330924
Chemicals, Peptides, and Recombinant Proteins		
OsO_4	Polyscience	Cat#23311-10
Ascorbic acid	Sigma	Cat#A4544
β-glycerophosphate	Sigma	Cat#G9422
Insulin	Sigma	Cat#I3536
Dexamethasone	Sigma	Cat#D2915
IBMX	Sigma	Cat#I7018
Rosiglitazone	Sigma	Cat#R2408
L-glutamine	Sigma	Cat#G7513
BPTES	Sigma	Cat#SML0601
O-(carboxymethyl)hydroxylamine hemihdrate (AOA)	Sigma	Cat#C13408
Bithionol	Sigma	Cat#SML1440
glutathione reduced ethyl ester	Sigma	Cat#G1404
dimethyl α-ketoglutarate	Sigma	Cat#34963
(U-^{13}C)glutamine	Sigma	Cat#605166
($^{15}N_2$)glutamine	Sigma	Cat#486809
L-(2,3,4-^{3}H)-Glutamine	American Radiolabeled Chemicals, INC	Cat#ART0149a
Critical Commercial Assays		
in-situ Cell Death Detection Kit, Fluorescein	Roche	Cat#11684795910
one-step NBT/BCIP solution	Thermofisher	Cat#PI34042
Clarity ECL substrate	BioRad	Cat#1705060
SuperSignal West Femto substrate	ThermoFisher	Cat#PI34095
Experimental Models: Cell Lines		
Mouse: ST2	http://cellbank.brc.riken.jp	RRID: CVCL_2205
Experimental Models: Organisms/Strains		
Mouse: $Gls^{fl/fl}$: $Gls^{tm2.1Sray}$/J	The Jackson Laboratory	RRID: IMSR_JAX:017894
Mouse: Prx1Cre: B6.Cg-Tg(Prrx1-cre)1Cjt/J	The Jackson Laboratory	RRID: IMSR_JAX:005584

(*Continued on next page*)

Continued

REAGENT or RESOURCE	SOURCE	IDENTIFIER
Mouse: BglapCre: B6N.FVB-Tg(BGLAP-cre)1Clem/J	The Jackson Laboratory	RRID: IMSR_JAX:019509
Mouse: LeprCre: B6.129(Cg)-*Lepr*$^{tm2(cre)Rck}$/J	The Jackson Laboratory	RRID: IMSR_JAX:008320
Mouse: Wild Type: *C57Bl/6J*	The Jackson Laboratory	RRID: IMSR_JAX:000664
Mouse: *Rosa26*^{tdTomato}: B6.Cg-Gt(ROSA)26Sor$^{tm9(CAG-tdTomato)Hze}$/J	The Jackson Laboratory	RRID: IMSR_JAX:007909
Oligonucleotides		
Primers for mouse β-actin, see Table S4	https://www.idtdna.com/	N/A
Primers for mouse Akp2, see Table S4	https://www.idtdna.com/	N/A
Primers for mouse Ibsp, see Table S4	https://www.idtdna.com/	N/A
Primers for mouse Bglap, see Table S4	https://www.idtdna.com/	N/A
Primers for mouse Pparg, see Table S4	https://www.idtdna.com/	N/A
Primers for mouse Cepba, see Table S4	https://www.idtdna.com/	N/A
Primers for mouse Sp7, see Table S4	https://www.idtdna.com/	N/A
Primers for mouse Runx2, see Table S4	https://www.idtdna.com/	N/A
Primers for mouse Fabp4, see Table S4	https://www.idtdna.com/	N/A
Primers for mouse Gls, see Table S4	https://www.idtdna.com/	N/A
Primers for mouse Gls2, see Table S4	https://www.idtdna.com/	N/A
Primers for mouse Gls2 (Gls2-1), see Table S4	Velletri et al., 2013	N/A
Software and Algorithms		
Image J	https://imagej.nih.gov/ij/	N/A
Graphpad Prism 6 software	https://www.graphpad.com/	N/A
Other		
α-MEM	ThermoFisher	Cat#12561-056
Glutamine Free α-MEM	Corning	Cat#15-012-cv
AG 1-X8 polyprep anion exchange column	BioRad	Cat#7316212
RNAeasy kit	Qiagen	Cat#79254
iScript cDNA synthesis kit	BioRad	Cat#1708841
SsoAdvanced SYBR Green	Biorad	Cat#1725275

CONTACT FOR REAGENT AND RESOURCE SHARING

Further information and requests for reagents may be directed to and will be fulfilled by the Lead Contact, Courtney Karner (courtney.karner@duke.edu).

EXPERIMENTAL MODEL AND SUBJECT DETAILS

Mouse Strains

Gls^{flox} (RRID: IMSR_JAX:017894), *Prx1Cre* (RRID: IMSR_JAX:005584), *BglapCre* (RRID: IMSR_JAX:019509), and *LeprCre* (RRID: IMSR_JAX:008320) mouse strains are as previously described (Masson et al., 2006; Logan et al., 2002; Zhang et al., 2002; DeFalco et al., 2001). *C57Bl/6J* (RRID: IMSR_JAX:000664) and *Rosa26tdTomato* (RRID: IMSR_JAX:007909) mouse strains were obtained from the Jackson Laboratory. We backcrossed all mice for 5 generations onto the C57Bl/6J background prior to experiments. Mice were housed at 23°C on a 12 hour light/dark cycle with free access to water and PicoLab Rodent Diet 20 (LabDiet #5053, St. Louis, MO). Mice were analyzed at 4 months of age and both male and female mice were analyzed. The assessment of all animal studies were performed in a blinded and coded manner. The Animal Studies Committee at Duke University approved all mouse procedures.

Primary Cells and Cell Lines

Primary bone marrow skeletal stem cells (SSC) were isolated from 2–4-month-old male and female mice. The ST2 cell line (RRID: CVCL_2205) was obtained from RIKEN. ST2 cells were originally established from long-term bone marrow cultures of BALB/c mice, the sex of which is unknown. Cells were maintained in ascorbic acid free aMEM containing either 15% FBS for primary SSC or 10% FBS for ST2 cells. All cell culture experiments were carried out at 37°C and 5% CO_2.

METHOD DETAILS

Mouse Analyses

Radiographs of mouse skeleton were generated using a Faxitron X-ray system (Faxitron X-ray Corp) with 20-second exposure under 25 kV. Micro computed tomography (VivaCT 80, Scanco Medical AG) was used for three-dimensional reconstruction, and quantification of bone parameters (threshold set at 320) from 200 slices underneath the growth plate. For OsO_4 μCT, bones were decalcified in 14% EDTA for 2 weeks. Adipocytes were stained using OsO_4. Micro computed tomography (VivaCT 80) was used for three-dimensional reconstruction, and quantification of adiposity (threshold set at 550) from 200 slices underneath the growth plate (Scheller et al., 2014). Bone histomorphometry was performed on femurs fixed in 10% buffered formalin overnight at 4°C followed by 2-week decalcification in 14% EDTA. Following decalcification, bones were embedded in paraffin and sectioned at 5 μm thickness. Hematoxylin and eosin (H&E), tartrate-resistant acid phosphatase (TRAP), and Picrosirius Red/Alcian Blue (AB/PSR) staining were performed following standard protocols. For dynamic histomorphometry, mice were injected with calcein (20mg/kg) intraperitoneally at 7 and 2 days prior to sacrifice respectively. Freshly isolated bones were sucrose embedded in OCT for fresh unfixed frozen sections using cryojane. Both static and dynamic histomorphometry were quantified using ImageJ (Egan et al., 2012). Briefly, photomicrographs were used to generate image masks representing bone and non-bone tissue. The images were used to quantify osteoblast and osteoclast numbers, bone surface, mineralizing surface, and interlabel width in Image J. Immunostaining was performed on 5μm paraffin sections for osteocalcin (OCN) and BrdU or 10μm frozen non-decalcified sections for perilipin (PLIN). For OCN and BrdU immunostaining, antigen retrieval was performed by incubating tissue sections in 10μg/ml proteinase K for 10 minutes followed by incubation in 3% H_2O_2 (v/v in Methanol) for 10 minutes to block endogenous peroxidase activity. Antibodies against BrdU (RRID: AB_10986341, 1:1000 dilution), OCN (RRID: AB_1587337, 1:500 dilution) or Perilipin (RRID: AB_10829911, 1:200 dilution) were used. TUNEL staining was performed using the in-situ Cell Death Detection Kit, Fluorescein. All Image analysis was performed in a blinded and coded manner.

Cell Culture

Primary bone marrow skeletal stem cells (SSC) were isolated as follows. Briefly, the diaphyses of the femur and tibiae were isolated and all extemporaneous tissue was removed. The epiphyses were removed and marrow was collected by centrifugation. Red blood cells were lysed and cells were washed one time before plating. For colony forming efficiency assays, $1x10^6$ SSC were plated in a T25 flask. 3 hours after plating, non-adherent cells were removed by washing vigorously with media. Cells were then cultured for 14 days as indicated for CFU-F and CFU-Ap assays. After 14 days, colonies were switch to either adipogenic media (CFU-Ad) or osteogenic media (CFU-Ob) for an additional 14 days. For high density cultures, SSC were plated and washed after 3 and 6 days to remove non-adherent cells. SSC were passaged at day 7 and all experiments were carried out at a seeding density of 21,000 cells/cm^2. Osteoblast differentiation was initiated when cells were 95% confluent by replacing the medium with α-MEM supplemented with 50 mg/ml ascorbic acid and 10 mM β-glycerophosphate for the indicated time period with a change of media every 48 hours. Mineralization was assessed by von Kossa or alizarin red staining. Alkaline phosphatase staining was performed using the one-step nitro-blue tetrazolium (NBT) and 5-bromo-4-chloro-3′-indolyphosphate p-toluidine salt (BCIP) solution. Adipocyte differentiation was initiated 3 days after cells reached confluency by replacing the medium with α-MEM supplemented with 1.7μM Insulin, 1μM Dexamethasone and 0.5 mM IBMX for three days. Media was then replaced with α-MEM supplemented with 1.7μM Insulin only for 4 days with a change of media every 48 hours. Adipogenic media for CFU-Ad assays also contained 1μM Rosiglitazone. Lipid droplets were visualized by Oil Red O staining. In the indicated experiments, glutamine free α-MEM was supplemented with 2mM L-glutamine, 10μM BPTES, 200μM O-(carboxymethyl)hydroxylamine hemihdrate (AOA), 7.5μM Bithionol, 1mM glutathione reduced ethyl ester, or 1mM dimethyl α-KG.

Mass Spectrometry Analysis of Glutamine Metabolism

SSC were cultured to confluency in 6cm plates prior to initiation of treatment. SSC were either treated with BPTES for 1 hour or were cultured for 7 days in either growth media or osteogenic media prior to incubation in 2mM (U-^{13}C)glutamine for up to one hour. At the end of the incubation, cells were washed with cold PBS and extracted 3 times with -80°C methanol on dry ice. The methanol extract was spiked with 20 nmol norvaline as an internal standard and centrifuged at 2000 × g force for 30 minutes after vortex. The supernatant was completely dried by N_2 gas. A modified GC-MS method was used for small polar metabolites assay (Wang et al., 2018). The dried residues were resuspended in 25 μL of methoxylamine hydrochloride (2% (w/v) in pyridine) and incubated at 40°C for ninety minutes on a heating block. After brief centrifugation, 35 μL of MTBSTFA + 1% TBDMS was added, and the samples were incubated at 60°C for thirty minutes. The derivatized samples were centrifuged for five minutes at 20000 x g, and the supernatants were transferred to GC vials for GC-MS analysis. The injection volume was 1 μL, and samples were injected in split or splitless mode depending on analyte of interest. GC oven temperature was held at 80°C for two minutes, increased to 280°C at 7°C/min, and held at 280°C for a total run time of forty minutes.

GC-MS analysis was performed on an Agilent 7890B GC system equipped with a HP-5MS capillary column (30 m, 0.25 mm i.d., 0.25 μm-phase thickness; Agilent J&W Scientific), connected to an Agilent 5977A Mass Spectrometer operating under ionization by electron impact (Meister, 1975) at 70 eV. Helium flow was maintained at 1 mL/min. The source temperature was maintained at 230°C, the MS quad temperature at 150°C, the interface temperature at 280°C, and the inlet temperature at 250°C. Mass spectra were recorded in selected ion monitoring (SIM) mode with 4 ms dwell time.

GSH and GSSG Labeling Analysis by LC-MS/MS

The method was modified from our previous LC-MS/MS method (Kombu et al., 2009). Cell pellet samples were treated with 10 mM N-Ethylmaleimide (NEM), sonicated for 1 minute, then add 250 μl MeOH, centrifuge for 15 minutes, dry the samples completely. Redissolve the dried residue in 50 μl H_2O and transferred to LC-MS vials for analysis.

A Sciex QTRAP 6500+ (Sciex, Ontario, Canada) equipped with trubo elextrospray ion source was operated under positive ionization mode. The UPLC system consisted of an ExionLC AD autosampler, a column oven, and gradient pumps. A Phenomenex Aeris PEPTIDE 1.7 μM XB-C18 column (50×2.1 mm, Torrance, CA) was selected for GSH and GSSG separation. The column was kept at 45°C. The GSSG and GSH were separated by a gradient elution. Mobile phase A was 0.1% formic acid in water-acetonitrile (98:2, vol/vol), and mobile phase B was 0.1% formic acid in acetonitrile-water (98:2, vol/vol). The flow rate was 0.4 ml/min.

Glutaminase Activity Assay

Primary cells cultured to confluency were incubated in α-MEM media containing 5mM glucose and 2mM glutamine for 12 hours prior to the experiment. Cells were washed 3 times with Hanks Buffered Saline Solution (HBSS) and cultured for 20 minutes in α-MEM media containing 5mM glucose, 2μM Glutamine and 4 μCi/mL L (2,3,4-^{3}H)-Glutamine. Glutaminase activity was terminated by washing 3 times with ice cold HBSS and scraping cells in 1mL ice cold milliQ water. Cells were lysed by sonication for 1 minute with 1 second pulses at 20% amplitude. After clarification, cell lysates were bound onto AG 1-X8 polyprep anion exchange columns. Uncharged glutamine was eluted with three 2mL volumes of water. Glutamate and downstream metabolites were eluted with three 2mL volumes of 0.1M HCl. Eluent fractions were pooled and combined with 4mL scintillation cocktail and DPM was measured using a Beckman LS6500 Scintillation counter.

RNA Isolation and qPCR

Total RNA was isolated from cultured cells using the RNAeasy kit with on-column DNase treatment. Reverse transcription was performed using 400ng total RNA with the iScript cDNA synthesis kit. Reactions were set up in technical and biological triplicates in a 96 well format on an ABI QuantStudio 3, using SYBR green chemistry. The PCR conditions were 95°C for 3 min followed by 40 cycles of 95°C for 10s and 60°C for 30s. Gene expression was normalized to *Actb* mRNA and relative expression was calculated using the $2^{-(\Delta\Delta Ct)}$ method. Primers were used at 0.1 μM, and their sequences are listed in Table S4. PCR efficiency was optimized and melting curve analyses of products were performed to ensure reaction specificity.

Western Blotting

Cells were scraped in lysis buffer containing 50 mM Tris (pH 7.4), 15 mM NaCl, 0.5% NP-40, and a protease inhibitor mix. Protein concentration was estimated by the BCA method. Protein (20 μg) was resolved on 4%-15% polyacrylamide gel and subjected to immunoblot analyses using the following antibodies. Antibodies against GLS (RRID: AB_2110382), Cyclin D1, (RRID: AB_2228523), Cyclin D3 (RRID: AB_2070801), α-tubulin (RRID: AB_2210548), AMPK (RRID: AB_330331), P-T172 AMPK (RRID: AB_330330), Eif2α (RRID: AB_10692650), PS51 Eif2α (RRID: AB_2096481), Chop (RRID: AB_2089254), Atf4 (RRID: AB_2058752) and β-actin (RRID: AB_330288) were used to detect the respective protein levels. All primary antibodies were diluted 1:1000 in blocking solution (5% milk, 0.1% Tween in TBS). The immunoblots were blocked for one hour at room temperature in 5% milk (TBS, 0.1% Tween) followed by an overnight incubation at 4°C in their respective diluted primary antibody solutions. Membranes were then washed three times using TBS/Tween 0.1% and further incubated with the secondary antibody, HRP goat anti-rabbit (RRID: AB_2099233) or HRP anti-mouse (RRID: AB_330924) in 5% milk (TBS/Tween 0.1%) for 1 hour at room temperature. All secondary antibodies were diluted 1:2000 in blocking solution. All blots were developed using either the Clarity ECL substrate or the SuperSignal West Femto substrate. Each experiment was repeated for a minimum of three times with three independently prepared protein samples.

QUANTIFICATION AND STATISTICAL ANALYSIS

Statistical analyses were performed using Graphpad Prism 6 software. All data are shown as mean values ±SD. In cell culture studies, statistical significance was determined by an unpaired 2-tailed Student's t-test. For uCT and CFU studies statistical significance was determine by a paired 2-tailed Student's t-test comparing paired littermate controls. Data were normally distributed as determined using the Komogorov-Smirnov test. A P value of less than 0.05 is considered statistically significant. Statistical parameters, including the value of n, are noted in the figure legends. Unless otherwise noted, all experiments were performed on 3 individual samples.